Seventh Quarterly Progress Report

July 1, 2003, through September 30, 2003

Speech Processors for Auditory Prostheses

NIH Contract N01-DC-2-1001

submitted by

Charles C. Finley
Punita Christopher
University of North Carolina at Chapel Hill
Department of Otolaryngology
Chapel Hill, NC

Donald K. Eddington
Massachusetts Institute of Technology
Research Laboratory of Electronics
Cambridge, MA

Barbara Herrmann
Massachusetts Eye and Ear Infirmary
Boston, MA

1.0 Introduction

Work performed with the support of this contract is directed at the design, development, and evaluation of sound-processing strategies for auditory prostheses implanted in deaf humans. The investigators, engineers, audiologists and students conducting this work are from four collaborating institutions: the Massachusetts Institute of Technology (MIT), the Massachusetts Eye and Ear Infirmary (MEEI), Boston University (BU) and the University of North Carolina at Chapel Hill (UNC-CH). Major research efforts are proceeding in four general areas: (1) developing and maintaining a laboratory-based, software-controlled, real-time stimulation facility for making psychophysical measurements, recording field and evoked potentials and implementing/testing a wide range of monolateral and bilateral sound-processing strategies, (2) refining the sound processing algorithms used in current commercial and laboratory processors, (3) exploring new sound-processing strategies for implanted subjects, and (4) understanding factors contributing to the wide range of performance seen in the population of implantees through electrical artifact, psychophysical, evoked-response and fMRI measures.

This quarter's effort was directed at six specific activities including: (1) studies of sound localization and speech reception in the presence of multiple noise sources using asynchronous sound-processing systems, (2) initiation of preparations to conduct similar experiments using synchronized sound processors, (3) continued monitoring of the binaural relationships of pitch, fusion, interaural time and just noticeable differences (ITD-JND), and binaural interactions in electrically-evoked brainstem responses, (4) fitting of additional chronic study subjects wearing CIS-based processors whose channel interactions have been minimized using triphasic pulses, (5) continued measurement and analysis of intracochlear evoked potentials (IEP) to assess variability of responses across subjects and to provide an objective measure of channel interactions, and (6) completion of initial studies to test device function using surface artifact potentials. In this QPR, we concentrate on the last activity, which involves the measurement and analysis of electrical artifact potentials from scalp electrodes in order to evaluate the functional operation of a cochlear implant under normal operating conditions.

2.0 Device Evaluation using Surface Artifact Potentials

A major objective of the current contract is to better understand the basis for variability in speech-reception outcomes across patients, especially in patient groups using the same cochlear implant device and sound-processing strategy. We hypothesize that these differences arise principally from variations in (1) the degree to which the sound-processing strategy was optimized for the patient, (2) the condition and position of the electrode array, and (3) the anatomical/physiological state (both central and peripheral) of the implantee. Implicit in these hypotheses is the assumption that the implanted receiver/stimulator is functioning properly and that the intended stimulus patterns are indeed being delivered to the implanted electrode array. One goal of our work is to develop techniques for objectively testing this assumption by examining device function

in individual implant subjects through analysis of electrical artifact potentials appearing on the scalp. By 'device function' we mean operation of the total prosthesis system including electrode array, implanted stimulator, external speech processor hardware, and software that implements the coding strategy. Malfunction of external components is readily addressed by equipment replacement, whereas evaluation of implanted hardware is difficult. Our approach is to examine operation of the total system and in the process identify deficient subcomponents.

This report summarizes our general approach to achieve this goal and describes our initial efforts to develop techniques, collect data and perform analyses. While the results reported are preliminary, they do provide insight into the level of detail that can be obtained and the various factors that must be considered in gathering accurate data and appropriately analyzing its significance. The emphasis in this report on delivery of charge balanced stimulation is only one component of a more general analysis plan described in Section 2.1 Before continuing with its description, we briefly address implant reliability and possible failure modes.

The most extreme form of malfunction is a complete failure in which the implanted device does not generate stimuli (e.g., a communication link cannot be established with the device or the device does not deliver stimulation when commanded). Such failures, commonly referred to as hard failures, are easily detected and typically require reimplantation (Kileny, Meiteles, Zwolan and Telian, 1995; von Wallenberg and Brinch, 1995). Common failures of such devices, as determined by manufacturers by destructive testing, include (1) electronic component failure, (2) mechanical failure of the hermetically-sealed case, (3) leakage around the electrical feed-through terminals of the case, or (4) fracture of the component substrate within the case. The frequency of occurrence of hard failures in cochlear implants is inconsistently reported. Some reports describe the percentage of patients who have experienced a hard failure compared to the total number of patients similarly treated at the clinical center (Kileny, Meiteles, Zwolan and Telian, 1995; Buchman, Higgins, Cullen, and Pillsbury, 2003). This statistic provides no information about duration of use before failure. Lehnhardt, von Wallenberg and Brinch, 2000 have described the reliability of the Nucleus device in terms of cumulative survival percentage, which is the percentage of devices surviving until a certain device age (99.2% at 1 year; 96.6% at 5 years; 95.3% at 10 years).

In contrast, malfunctioning devices that continue to deliver stimuli in response to input commands, but in an inappropriate manner, can be difficult to identify (von Wallenberg and Brinch, 1995; Battmer, Gnadeberg, Lehnhardt and Lenarz, 1994; Kileny, Meiteles, Zwolan and Telian, 1995; Stoddart and Cooper, 1999). Such conditions are often referred to as soft failures. Classes of such failures include intermittent function, open/shorted electrodes, generation of odd percepts, and/or inappropriate stimulation during system power up and shut down transitions. In many cases, these soft failures are apparent to the user in terms of altered percepts and/or to the clinician in terms of objective fitting/testing measures or patients' anecdotal reports. Malfunctioning devices that deliver stimuli with a distorted representation of the intended information are much more difficult to detect and may limit and/or reduce the user's speech reception

performance. In these cases, it is often difficult or impossible for the clinician or user to identify the device as a limiting factor. The incident of 'soft' failures is not known. A recent study (Buchman, Higgins, Cullen, and Pillsbury, 2003) reported on one center's experience where 13% (30) of implanted adult patients (224) underwent revision surgery because of auditory or non-auditory symptoms and/or performance-related issues that suggested device involvement. Of these cases eight (27% of revised cases; 3.6% of all patients) were 'hard' failures due to loss of communication lock with the device. Another five (17% of revised cases) devices were found through the manufacturer's device analysis to have various hardware and electrode failures present despite the ability of the device to stimulate and maintain lock prior to revision. For the remaining eighteen (60% of revised cases) devices that were removed and examined by the manufacturer, no hardware problems were identified**.** This study reported that revision surgery had a 90% success rate with patients no longer having the symptoms they had prior to revision surgery as well as benefiting from significant improvements in outcome. This high improvement rate, coupled with the relatively high rate of finding no device problems on examination, suggest that other medical/patient factors may be involved and/or better device assessment tools need to be employed.

Pediatric implantation poses even greater device integrity and associated diagnostic problems due to the active lives of young children and their less mature reporting abilities (Cullington and Clarke, 1997; Luetje and Jackson, 1997; Garnham, Cope and Mason, 2000). Hard failure rates in children are greater than those in adults, primarily due to more frequent occurrences of physical impact damage to the device (personal communications with clinicians and manufacturers). A reasonable hypothesis would be that device trauma may initiate a 'soft' failure condition (e.g. a case crack causing loss of hermiticity and allowing moisture to contact the electronics) which in turn leads to a 'hard' failure condition either immediately or progressively over time. One might anticipate then that an elevated number of 'soft' failures may occur among pediatric users, in addition to the expected rate of spontaneous soft failures.

A number of investigators have described techniques for assessing device function in patients. These techniques include measurement of surface artifact potentials (Carter, 2001; Cullington and Clarke, 1997; Garnham et al., 2000; Heller, Brehm, Sinopoli and Shallop, 1991; Kileny et al, 1995; Mens, Ooostendorp and van den Broek, 1993 and 1994; Mens and Mulder, 2002; Shallop, 1993), recording of evoked neural potentials (Bordure, O'Donaghue, and Mason, 1996; Garnham et al., 2000; Kileny et al, 1995; Shallop, 1993; Shallop, Facer, and Peterson, 1999; Truy, Gallego, Chanal, Collet, and Morgon, 1998), and measurement of acoustic reflexes (Shallop, Facer, and Peterson, 1999). All of these approaches have proved useful in assessing device function in patients, but also have various limitations. All employ very specific *ad hoc* stimuli to examine particular features of device function, and all involve a relatively small number of stimulus events in the examination. In general, the device is not tested in its normal operational mode (e.g. driven by a sound processor with speech signals). Because of our emphasis on evaluating speech-processing performance, we have borrowed heavily from the preceding body of work in recording artifact potentials and have expanded the analysis to address broader ranges of cochlear implant operation.

2.1 General Approach

The present report describes our work to develop a generic approach for evaluating implanted cochlear prostheses during realistic speech processing. This approach is intended for the "*in situ*" monitoring of implanted devices in individual patients, independent of the type of manufactured device she or he may have. The general approach is outlined in Figure 1. Earlier reports of this work are contained in a master's thesis (Christopher, 2003) and a poster (Christopher and Finley, 2003).

In general, electric artifact potentials generated during stimulation by an implanted stimulator are recorded from the scalp and amplified to provide an indirect measure of multichannel electric stimuli. The implanted device under examination is activated and controlled by a standard clinical speech processor, just as the device would operate in normal use. The test input to the speech processor may be a representation of acoustic signals from a microphone or electric waveforms connected to the auxiliary input. An additional mode of stimulation uses direct software control of the speech processor to generate specific *ad hoc* stimuli (as in the case of psychophysical testing for device programming). This report focuses on results obtained by realistic speech stimuli delivered directly to the auxiliary input.

The two panels on the left side of Figure 1 show typical multichannel artifacts recorded from a MedEl patient in response to the presentation of the speech token /aba/. The patient's sound processor was programmed with a continuous interleaved sampling (CIS) coding strategy, which stimulates only one electrode channel at a time while scanning across all available channels in repeating sequential frames. The lower panel shows the scalp potential recorded during the 800 msec duration of the speech token. The recording includes a significant time segment before the leading /a/ of the /aba/ begins. The large magnitude of artifacts during this segment before the speech stimulus begins is most likely due to the AGC of the speech processor being in release, thus allowing low magnitude signals to pass uncompressed. Once the speech presentation begins, the AGC becomes active and larger magnitude stimuli are compressed by the AGC before being sampled by the speech processing algorithm.

The subsequent prosodic envelope features of the coded sound are clearly visible in the remaining artifact record. Two, high-energy vocalic portions of the utterance separated by the lower-energy consonant transition are shown. This record, sampled at a 200 kHz sampling rate, contains approximately 160,000 samples. During the displayed 800 msec interval, the speech processor has generated about 14,800 biphasic stimulus pulses. The upper panel expands the time scale and shows a 1.1 msec portion of the full record in which the electrical artifact elicited by the individual biphasic stimuli are easily seen. Each biphasic artifact begins with a negative-going initial phase, followed by a positive-going phase of approximately equal magnitude. The panel shows 20 biphasic stimuli (each with 27 μsec phase duration), which represent slightly more than two, full round-robin frames of multichannel stimulation by this 12-channel CIS processor. The irregular tops and bottoms of each artifact phase are due to high-frequency noise in the recorded.

signal.

The artifact records may be further processed so that the overall function and accuracy of the implanted device/speech processor combination under test may be evaluated. A computational model of the speech processor design was developed to provide predicted patterns of the output stimuli for each individual channel of stimulation. Individual channel outputs are also summed to provide a prediction of the multichannel artifact recording. Analytical software tools written in MatLab are used to decompose the multichannel artifact recordings into single channels of encoded information. The measured and predicted electrical artifact signals may be compared to examine device function. Deviations of the measured artifacts from predicted waveforms suggest either that the implant system is defective or that the real speech processor/stimulator system does not accurately implement the desired system design as characterized by the model. The consequence of either of these factors is that speech reception performance of an individual patient may be significantly diminished from what it might be. A key objective of this work is to identify this situation apart from the presence other patient-related factors such as electrode placement, neural survival, and/or central nervous system changes that may influence outcome. Data presented in this report are based on measures with the Advanced Bionics Corporation Clarion C-II and Med-El Combi-40 implant systems. Similar measures have also been made from Nucleus 24 patients.

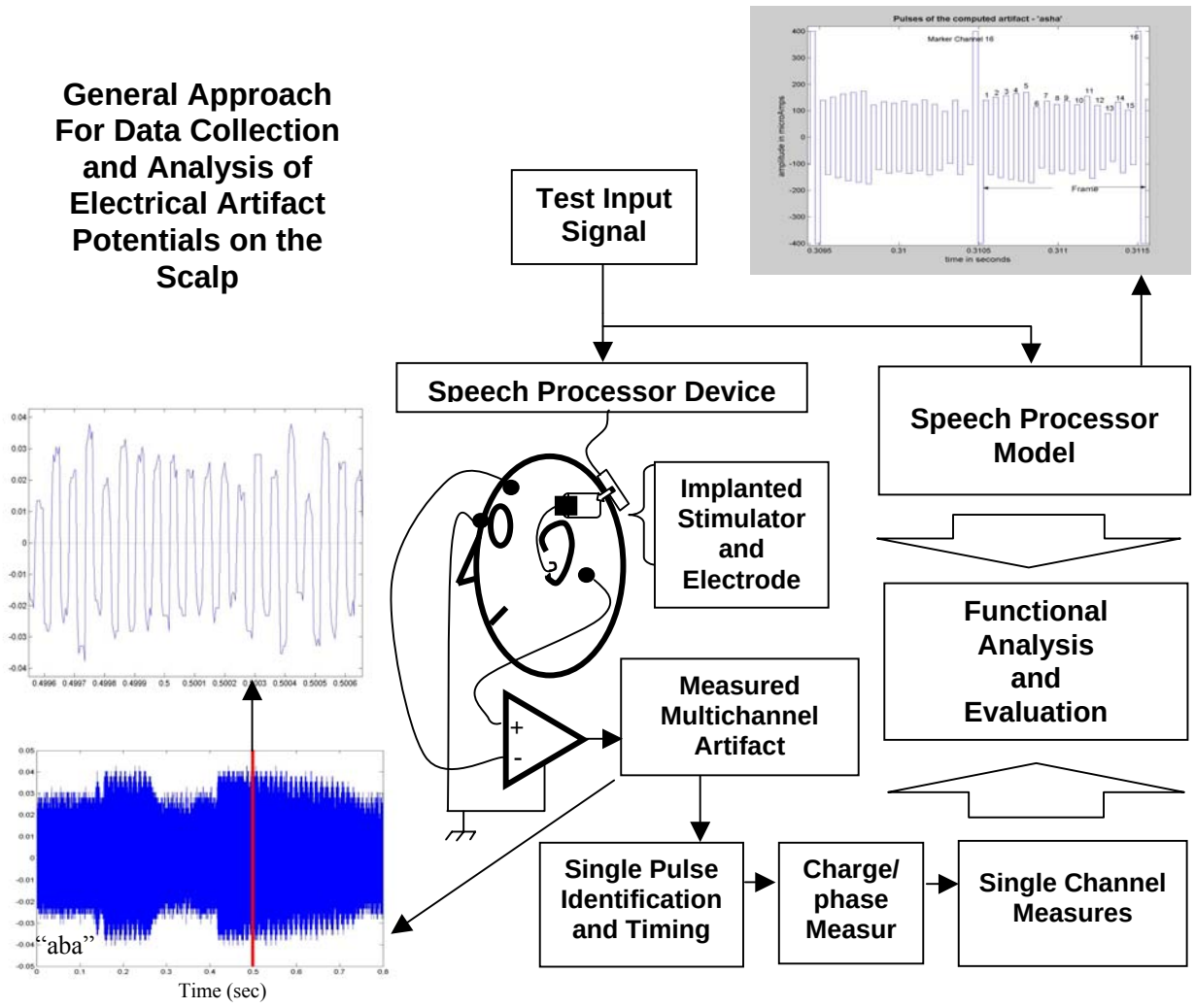

Figure 1. General approach for measurement and analysis of surface artifact potentials

2.2 Recording Methodology and Gross Examination of the Data

A custom hardware and software system was developed to facilitate synchronized stimulus presentation and recording of artifact potentials. The hardware includes a wide-bandwidth, fast-recovery, optically-coupled, differential bio-potential amplifier suitable for recording surface potentials using standard EEG recording electrodes. This unit is connected to a data acquisition card, which records ongoing artifact potentials under software control and also includes D/A outputs for generation of the input signals delivered to the sound processor. The software system for controlling signal presentation and recording was written in Visual Basic (VB) and features the capability to output a precomputed input-signal buffer while simultaneously sampling and storing data in a sampled data buffer at high speed (100–500 kHz sampling rate). Buffer lengths and sampling rates can be selected to produce single input-signal/recording epochs ranging from a few msec to several seconds in duration. The input signal was fed to the sound processor's auxiliary input (speech signal, swept sine wave, or an arbitrary synthesized waveform).

To facilitate software development, bench-level measures were made initially with implantable stimulation devices driving resistive loads. This was followed by measures of artifacts in a saline bath containing a fully immersed Clarion C-II stimulator and Hi-Focus electrode array. Once the basic methodology was developed and safety features of the hardware and software were tested, artifact data were obtained from patients using standard disposable EEG recording electrodes. Data presented here were collected at the Callier Cochlear Implant Center at the University of Texas at Dallas and at the University of North Carolina at Chapel Hill. Subsequent analysis of the records was performed with software tools developed using MatLab.

Multichannel Stimulation: Resistive Load For the resistive load studies, the Clarion Hi-Resolution Workbench software was used to set up a 16-channel sound processor with sequential, non-simultaneous CIS stimulation across channels. The workbench was used to set the Most Comfortable Level (MCL) and Threshold (THR) values for each channel, the pulse width of the stimulus pulses, and the channel gains of the processor system. Volume settings were fixed in the speech processor at mid range (typical of normal use by a patient). The AGC function was disabled in the Clarion bench tests, but was active with the MedEl patient testing described later. MCL and THR values as described in Table 1 were used to establish typical mapping levels for each channel. MCL and THR for channel 16 were both set to a single fixed value in order to generate a constant, large-magnitude artifact on a fixed channel to clearly define the completion of each stimulus frame in the artifact record.

Channel Num	THR	MCL
1-15	50	250
16	400	400

Table 1. Channel amplitude mapping parameters for test CIS sound processor

As shown in Figure 2, each output channel from a board-mounted, C-II current stimulator (left panel) was connected to a 5.1K-ohm load resistor, which terminated to a common current-summing node (right panel). This node connected to the stimulator common monopolar case ground through a single, 50-ohm resistor. The voltage appearing across the common resistor reflected the summed current from all output channels. With the sound processor running the CIS, the full sequential ordering of the multichannel output is visible at the summing node. Figure 3 shows this measured voltage for a 16-channel Hi-Resolution processor in response to a segment of the speech stimulus /aba/ (from the Iowa test battery). The figure shows large, constant-magnitude biphasic pulses due to stimulation on channel 16, separated by 15 smaller biphasic pulses of varying amplitudes due to stimulation on the remaining channels. Data were sampled (16-bit resolution) at a 400 kHz rate and saved for off-line processing.

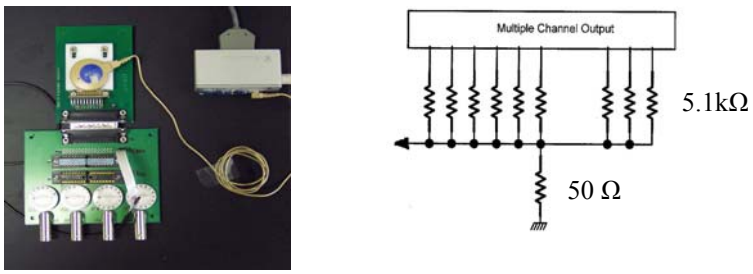

Figure 2. Clarion C-II multichannel stimulation into a resistive load

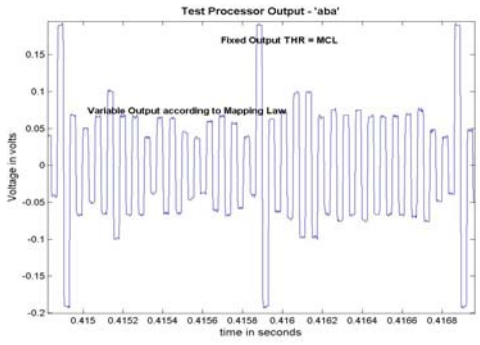

Figure 3. Multichannel processor outputs recorded at common summing node

Multichannel Stimulation: Saline Bath In this test condition, a Clarion C-II stimulator device with Hi-Focus electrode array was immersed in a saline bath as shown in Figure 4. A sound processor (top center) is coupled to the stimulator device with a transmitting headpiece placed below the bottom of the saline bath adjacent to the device. The cable leading from the stimulator to the Hi-Focus electrode and the electrode itself can be seen running vertically in the saline bath. Current passed from the contacts of the Hi-Focus electrode generate electrical fields in the volume of the bath. Potentials are differentially recorded from bare wire electrodes inserted into the bath at positions near the tips of the red (+) , blue (-) and black (gnd) probes in the photograph. The environment in the saline bath provided an electrode/fluid interface that resembled more realistic operating conditions than the resistive loads. Figure 5 shows a segment of a multi channel artifact record collected from this saline bath in response to the speech token /aba/. In this case, channel 16 is mapped for a typical dynamic range as opposed to being a fixed value. Very clean, well-defined artifacts are observed. The spontaneous zero magnitude event in the record (at time 0.1435) is of unknown origin

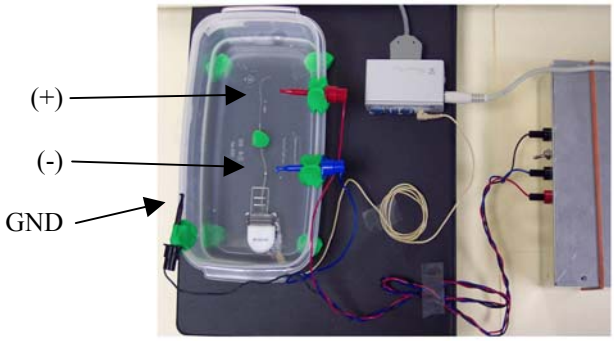

Figure 4. Saline bath with Clarion C-II stimulator with Hi-Focus electrode

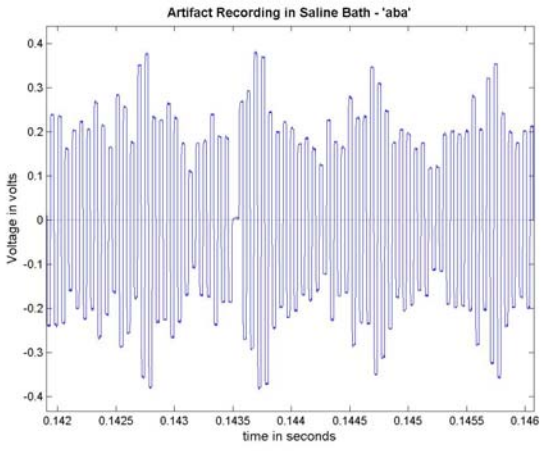

Figure 5. Artifact data obtained from the saline bath

Multichannel Stimulation: Implanted Patient Surface EEG electrodes were placed at C_z (+) and the contralateral mastoid (-) for Patients 2 and 4 or on ipsilateral mastoid (+) and the contralateral mastoid (-) for Patient 1 with a forehead ground reference for differential artifact recording (x10 amplification). Representative raw data records from three Med-El patients for presentation of /aba/ are shown in Figures 6, 7 and 8 below. The left panel of each figure shows the full 800 msec artifact record. The right panel's time scale is expanded and shows a brief segment taken from the full record. The data for Patient 1 in Figure 6 are the same data discussed earlier as part of Figure 1. These data are repeated here to provide a reference for examining the data from Patients 4 and 2, in that order.

The full artifact data record for Patient 4 (Figure 7 – left panel) is generally similar to that observed for Patient 1 (Figure 6) in showing the overall prosodic structure of the speech token /aba/. The right panel with expanded time scale reveals a different fine temporal structure with longer duration biphasic pulses separated by intervals of no stimulation. This output time structure is by design, being specified during clinical fitting of the implant system and implemented in the sound processor DSP code. This particular sound processor employs stimulation on 7 output channels processor and has aframe interval of 822 μsec [7 channels X (50 μsec/phase X 2 phases/channel + 26 μsec dead time between phases) = 822 μsec/frame ➔ 1133 Hz update rate per channel]. This is in contrast to Patient 1's 12-channel processor and running at a faster rate in Figure 6 [12 channels X (26 μsec/phase X 2 phases/channel + 0 μsec dead time between phases) = 624 μsec/frame ➔ 1603 Hz update rate per channel].

The artifact recordings for Patient 2 (Figure 8) are distinctly different from those for Patients 1 and 4. The full record shows the presence of (1) magnitude clipping during large-magnitude, positive-going artifacts and (2) overshoots occurring during large-magnitude, negative-going artifacts. The expanded time record in the right panel of Figure 8 illustrates some of these events at finer temporal resolution. Notice that the clipping event occurs in the leading cathodic phase of a biphasic stimulus and is followed by the overshoot phenomenon during the corresponding trailing phase. Detailed examination of the record also suggests that there may be some degree of asymmetry in the areas of the leading and trailing phases of some of the biphasic artifacts, as will be discussed later. This record also shows the presence of two artifacts with phase durations twice those of the other pulses. These longer duration stimuli appear as they should, being specifically coded into the patient's processor map. This sound processor employs stimulation on 12 output channels processor and has a frame interval of 720 μsec [10 channels X (26 μsec/phase X 2 phases/channel + 2 channels X (50 μsec/phase X 2 phases/channel) = 720 μsec/frame ➔ 1389 Hz update rate per channel].

Despite the presence of the odd stimulus artifacts, Patient 2, an adult user, reported no specific problems with the device and was maintaining stable performance with a "good" outcome.

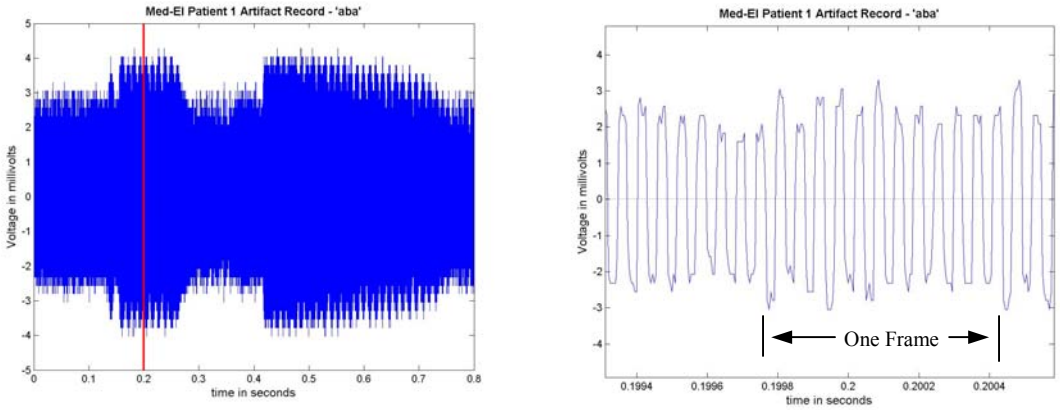

Figure 6. Med-El Patient 1 artifact data in response to /aba/

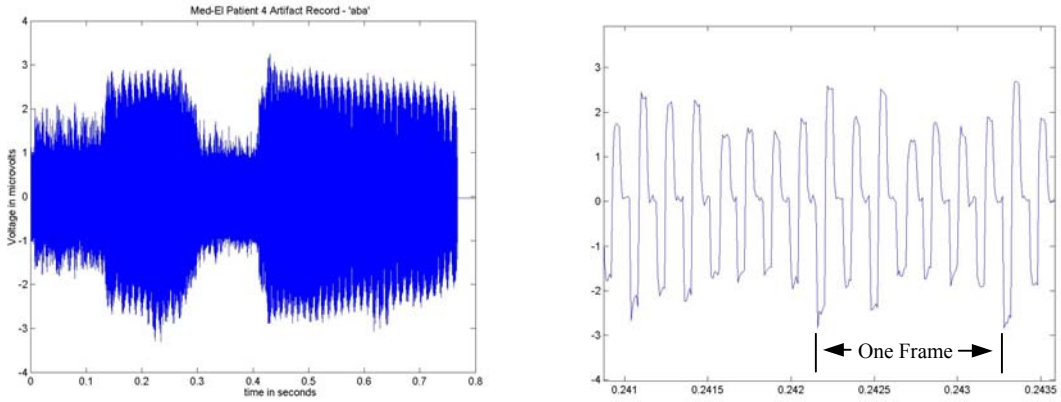

Figure 7. Med-El Patient 4 artifact data in response to /aba/

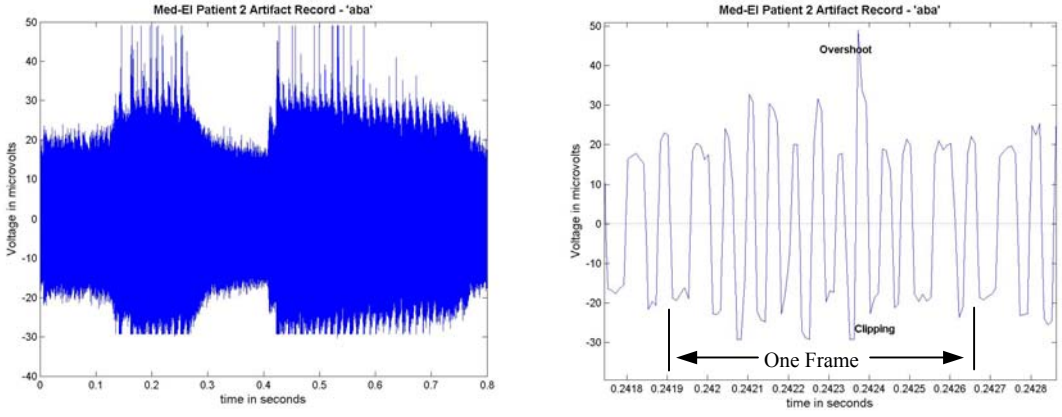

Figure 8. Med-El Patient 2 artifact data in response to /aba/

2.3 Characterization of Artifact Potentials on a Pulse-by-Pulse Basis

The gross examination of the artifact records presented above suggested that a channel-by-channel analysis of individual stimulus pulses would be helpful. In addition, automation of data analyses would enable screening of large numbers of stimulus events as opposed to performing visual spot checks on a few pulses. The remainder of this section describes an analysis procedure we are developing that is designed to break the artifact records containing thousands of stimulus events into individual stimulus phases sorted by stimulation channel. The process begins with identification of individual biphasic artifact events, followed by quantification of the magnitudes of the leading and following phase of each event, and ending with sorting of the stimulus events on a channel-by-channel basis.

Correlation Analysis to Identify Occurrence of a Biphasic Event in the Artifact Record
To identify individual biphasic artifacts, an artifact record was cross-correlated with a template of the interphase transition of a biphasic pulse as shown in Figure 9. High correlations occurred at the pulse transitions, as shown in Figure 10. MatLab software routines pick up these correlation peaks and determine the time in the artifact record when such an event occurred. The corresponding positive and negative artifact amplitudes are then determined and marked for visual examination of the record to check the accuracy of the analysis as shown in Figure 11.

The magnitude of the charge delivered by the stimulator was estimated by computing the area in each phase of the artifact. Areas for each phase are based on sums of the portions of artifact areas between sample values that contribute to each phase. In most cases this is the trapezoidal area formed by adjacent sample points. In the case of sample points between which a zero crossing occurs, the contributing area is the triangular region occurring within the phase as formed by a linear interpolation of the adjacent sample points. In Figure 12a these areas would be triangles CDE and FGA for the positive phase. Leading and trailing phase areas for each individual pulse are calculated and saved separately for later analysis.

Assuming that artifact magnitude is proportional to the current injected into the tissue, calculation of artifact phase areas (volts X time) provides an estimate of charge (amperes X time) injected during each phase. It is important to recognize the limitations of this assumption, however. In the case of potentials measured using the resistive load, the measures reflect true total current passing during stimulation and provide direct access to the amount of charge injection. However, in the case of artifact measures in the saline bath or in patients, the artifact magnitude can only be assumed to be proportional to the actual current being passed by stimulation and consequently provides a relative estimate of actual current. Note also that low-level currents at or below the measurement noise floor and passed over longer time periods will contribute significant amounts of charge transfer that the present analysis does not detect. This may be especially significant in the case of passive, long-term charge recovery that occurs following the delivery of a balanced, biphasic current pulse into a capacitive load.

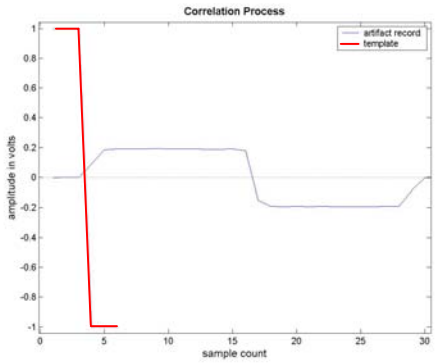

Figure 9. Cross-correlation template and artifact record on an expanded time scale

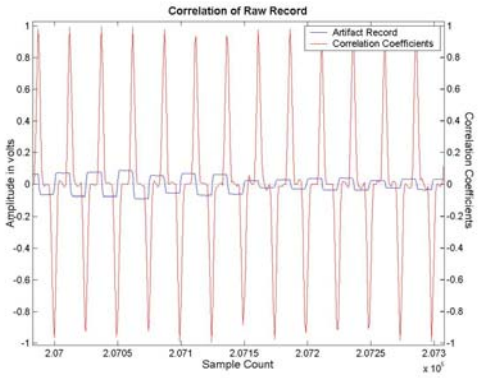

Figure 10. Cross-correlation result of template and artifact data

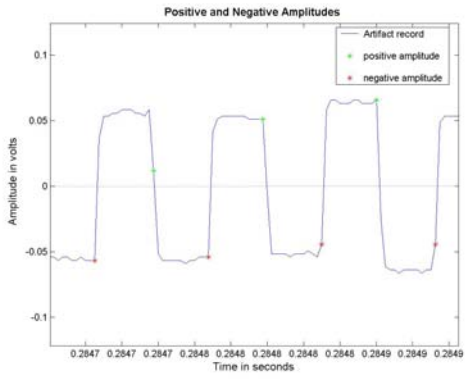

Figure 11. Artifact magnitudes at times associated with negative or positive peaks in the cross-correlation process of Figures 9 and 10. The biphasic artifacts in this case have positive leading phases.

For purposes of the following discussion, we will treat the calculated artifact areas (voltage X time) as rough estimates of stimulation charge pending additional refinements to the analysis such as stimulus/response averaging to reduce the masking effects of noise.

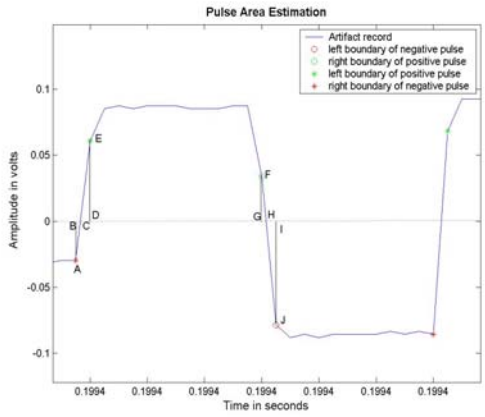

Figure 12. Phase area calculations example

2.4 Initial Analysis of Charge Balancing of Leading and Following Stimulus Phases

Charge Balancing Inferred by Areas of Artifact Phases This section compares the areas of the positive and negative phases of the individual biphasic pulses of the artifact record. Ordinarily electrical stimulation of tissue should have zero net charge; consequently, for a biphasic pulse the estimated charge would be expected to be equal for the leading and following stimulus phases.

The panels of Figure 13 illustrate the balancing of charge across all channels for (a) bench test measures, (b) Patient 1, (c) Patient 4, and (d) Patient 2, respectively. The bench test measures are from a Clarion device with resistive load (see Figures 2 and 3), while patient records are from patients using Med-El devices. Results are plotted as a scatter plot of the estimated charge of the positive (following) phase versus the estimated charge of the negative (leading) phase for all individual pulses across all channels for the speech stimulus. For instance, the scatter plot for Patient 1 (Figure 13b) includes approximately 14,800 points and shows data for 12 channels of stimulation.

Biphasic pulses that are charge balanced have equal charge in each phase and will fall along the major diagonal of the scatter plot as seen in Figure 13a. In this figure the small, isolated cluster of points with large charge magnitude is associated with the constant magnitude stimulation defined for channel 16 (see Figure 3 and Table 1). The results indicate that for the bench test measures with resistive loads, the pulses are symmetric in terms of charge magnitude. Additional measures are planned using bench versions of the MedEl and Nucleus stimulators with resistive loads.

In Figure 13b the charge across all channels for Patient 1 appears to be well-balanced, except for a slight tilt in the distribution of the data in favor of the estimated charge of the leading phase being less than the following phase at higher stimulus levels. This trend is demonstrated in the figure by the linear regression line for the aggregate data across all channels. At lower levels there appears to be a slight tendency in the opposite direction with the leading phase being larger than the following phase. The same behavior is seen also in Figure 13c in the data from Patient 4, although to a greater extent and with greater scatter in the aggregate data. Patient 4's processor stimulates on 7 channels and runs at a slower overall rate with 50 usec/phase pulses separated by 27 usec blank intervals (Figure 7). Consequently, fewer stimulus events are delivered (approximately 7,800) during the speech presentation.

In Figure 13d the data for Patient 2 are similar in some respects but show additional features compared to those from Patients 1 and 4. The scatter distribution shows a main central lobe with smaller lobes on each side. The main central lobe repeats the pattern seen in Figures 13b and 13c for Patients 1 and 4, respectively, with a slight counter-clockwise rotation in the scatter distribution. The side lobes are also a significant feature and have been examined in more detail since the first reporting of this figure (Christopher, 2003; Christopher and Finley, 2003). Our present understanding of these

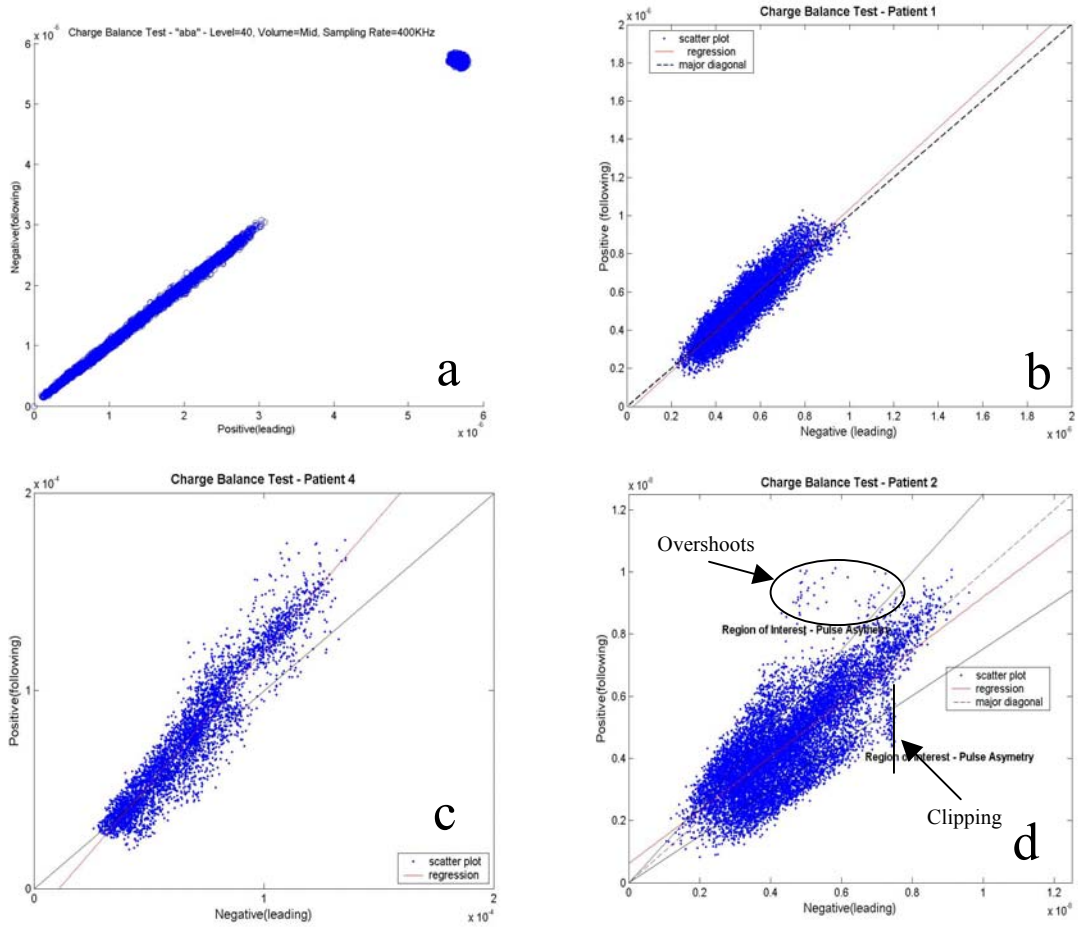

Figure 13. Scatter plots of artifact areas for leading and following phases across all channels for (a) C-II with pure resistive loads, (b) MedEl Patient 1, (c) MedEl Patient 4, and (d) MedEl Patient 2.

side distributions is that they are due to a computation artifact in calculating phase areas when the artifact sampling rate is too low to sufficiently characterize the brief contiguous phases of the artifact. In such situations, when one phase area is underestimated the other is overestimated, giving rise to the general symmetry in the side lobe scatter distributions on each side of the major diagonal. The linear regression line for the aggregate data in Figure 13d is tilted in a direction opposite to the previous data and may be biased by the anomalous side lobe data. This issue is continuing to be reviewed to ascertain the most appropriate sampling rates and recording bandwidths, especially for examining systems employing very brief phase durations (10 μsec/phase in the case of Clarion Hi-Resolution processors). It is anticipated that sampling rates of 500k samples/sec or faster will be more appropriate than the 100k–200k rates used for the present data.

The clipping and overshoot phenomena described in Figure 8 for Patient 2 are present in the Figure 13d scatter plot as well. Clipping is observed by the presence of an upper bound on the leading phase charge that can occur; whereas overshoots appear as a cloud

of events with large magnitude following phases that is located apart from the main data clusters. While Figure 8 (right panel) shows an example of large magnitude clipping and overshoot associated with the same pulse, it is clear from the scatter plot that clipping of large magnitude leading phases can be followed by second phases with a range of lower magnitudes. Likewise, the following phases with large magnitude overshoots can be preceded by a range of unclipped leading phases. The analysis software is being expanded to allow examination of the time representation of single specific pulses represented by points in the scatter plots to facilitate a more detailed analysis.

Before examining the scatter data for Patients 1 and 4 on a channel-by-channel basis, it is worth considering possible mechanisms associated with stimulation and artifact recording that may cause the linear regression line of the data to deviate from the major diagonal. In simple terms, this deviation may be considered as a summation of (1) a change in slope and (2) a shift in position as shown in Figure 14. Several mechanisms may be contributing at once, and the present analysis makes no attempt at decomposing the specific components in the data other than listing possibilities. While this simple analysis assumes a linear model, it is not meant to exclude the possibility of nonlinear effects in which devices behave non-ideally with their characteristics changing due to operating level and/or past history for example.

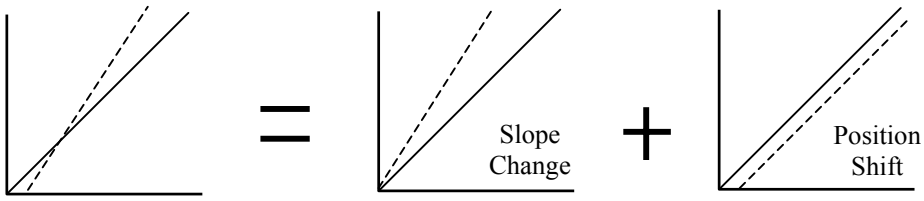

Figure 14. Decomposition of regression change into a slope change and position shift

Factors that may contribute to a slope change include, but may not be limited to:

- Caused by stimulation by the implanted device
  - Current source gain differences for positive and negative current stimulation;
  - Voltage compliance limiting in a current source as peak output voltage levels across the electrodes approach the power supply limits of the current source;
  - Exacerbation of the above voltage compliance limit issue if the average voltage across the output coupling capacitor grows with accumulation of non-zero net residual charge; and
  - Differences in voltage divider ratios created by different output impedances of the current source(s) for positive and negative stimulation in combination with variable electrode impedances.

Caused by recording of artifact potentials

- Distortion of the measured artifacts by recording with too low a bandwidth which results in (1) the leading phase being greater in magnitude than the following phase due to delayed transfer of charge and (2) generation of a low-magnitude, long-duration tail following the biphasic pulse (see Figure 15). This is effect is similar to the mechanism in which biphasic pulses may leave residual charge on capacitive neural membranes (see Eddington *et al*., 2002 – QPR1 of this project). Limited recording bandwidth in the recording pathway and excessive bulk shunt capacitance in the tissue could contribute to this distortion; and
- Failure of the present analysis techniques to account for the low magnitude, slow recovery following the biphasic artifact. The present technique detects the end of the following phase and ends charge estimation, neglecting the trailing component, which may be below the measurement noise floor.

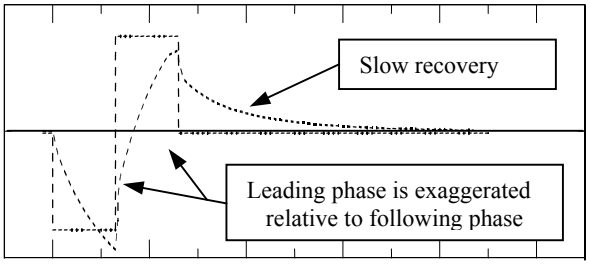

Figure 15. Distortion of leading- and following-phases of a biphasic pulse through a bandwidth-limited filter.

Factors that may contribute to a position shift include:

- Caused by stimulation by the implanted device
  - Presence of a constant current shunt in stimulator;
  - Steady DC offset in command control signal for current source; and
  - Missing or stuck bit in command stream.

- Caused by recording of artifact potentials
  - DC offset in recording path

Estimated Charge Balancing in Individual Channels Figures 16 and 17 show the data of multichannel scatter plots Figures 13b and 13c plotted for individual channels for Patient 1 and Patient 4, respectively. Each figure shows multiple panels with one for each active stimulation channel of the patient's speech processor. The channels and corresponding panels number from left to right beginning with the top row so that channel 1 is in the upper left-hand corner and the last channel is at the rightmost end of the lower row. Each

panel also contains the linear regression line for the pulses present by that channel of stimulation.

Figure 16 shows that the leading- and following-phase scatter distribution of artifact charge magnitude for each of Patient 1's stimulation channels lie generally along the major diagonal. This is consistent with the plot for all data in Figure 13b, where the linear regression line deviates with a slight counterclockwise rotation from the major diagonal. In contrast, deviations of regression lines for individual channels in Figure 16 occur in either direction and to varying degrees across channels. Because the MedEl system uses a single current source multiplexed across channels, the involvement of channel specific factors (possibly impedance) is thus suggested. Another observation across channels is that the ranges of charge magnitudes vary. For instance in the rightmost column of Figure 16 the data range is the most for channel 4 (top-right) and the least for channel 12 (bottom-right), with the range for channel 8 (middle-right) being intermediate. This variation is most likely due to a combination of several factors including: (1) different maps for each channel based on psychophysically fitted THR and MCL values, (2) different ranges of coded energy for each channel based on the spectral energy distribution for the speech token, (3) differences across channels in the magnitude of generated surface artifacts due to variation in electrode interface impedances, and (4) anatomical factors influencing electrical field spread from each stimulating electrode site to the recording electrode.

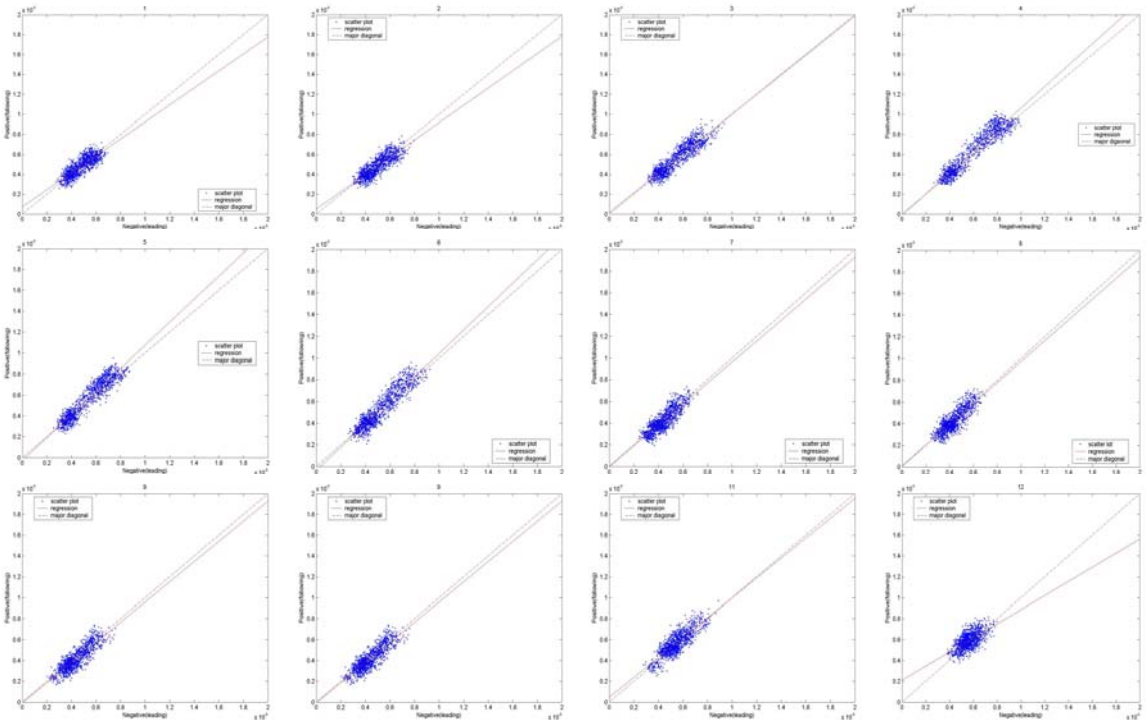

Figure 16. Scatter plots of estimated charge for individual channels of the 12–channel processor of Patient 1

Figure 17 shows similar individual channel scatter data for Patient 4. In this case, variation in the ranges of the data is seen across channels also. Deviation of the linear regression for each channel is much larger and more consistent across channels with the exception of the last channel (#11).

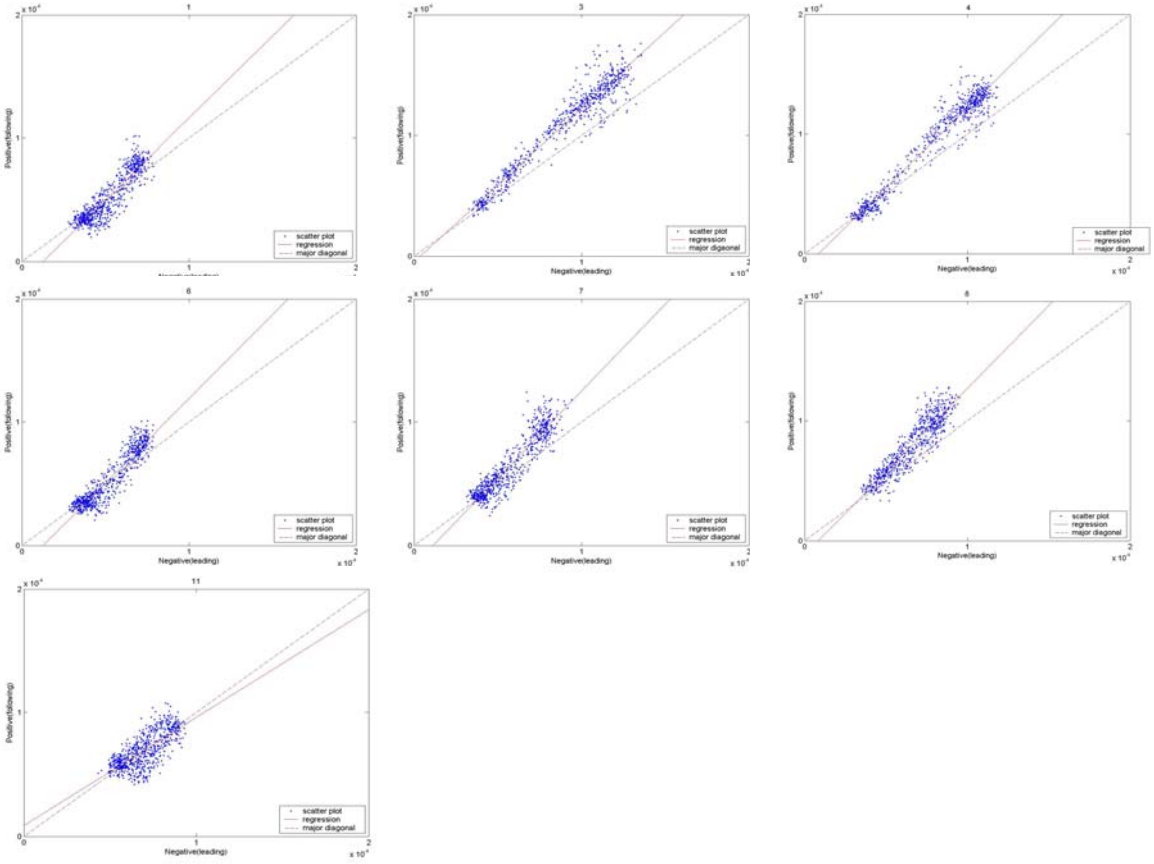

Figure 17. Scatter plots of estimated charge for individual channels of the 7–channel processor of Patient 4

Summary of Patient Results on Estimated Charge Balancing

The large differences between the negative-phase vs. positive-phase plots for Patients 1 and 4 indicate the two devices differ significantly in the stimuli delivered for the same input waveform. The clipping associated with Patient 2 is not seen in Patient 1 or 4, although some of the overshoot behavior noted in Patient 2 is present in Patient 4 (see Figure 7, left panel at times 0.24 and 0.64 sec).

While the biphasic pulses delivered to these patients show evidence of estimated charge imbalance, this does not necessarily mean that a net DC charge is being delivered during use of the device. The MedEl system includes coupling capacitors on each electrode lead

designed to insure delivery of zero net charge. When a biphasic pulse is delivered with asymmetric currents in each phase (most likely what the artifact measures reflect), the resultant effect is that at the end of the trailing phase a residual charge is left on the coupling capacitor that is passively discharged back into the tissue over a long time span. The long-term effect is zero net charge injection. The short-term effect, especially if repeated by many stimuli in a short time span, is an accumulation of charge on the coupling capacitor, which produces a residual voltage on the capacitor. This voltage in turn reduces the effective voltage compliance range of the current source, which limits the ability of the stimulator to deliver the requested current amplitude (and may be one reason for clipping observed in Patient 2. The patient may or may not recognize this deviation as a distinct acoustic precept, but may have lost or misinterpreted the intended coded information nevertheless.

The ability to detect such situations as a contributing factor in determining individual patient outcomes is the object of our effort to evaluate device performance using surface artifact potentials. This work is continuing with collection of data from a wider range of patients implanted with all devices. In addition, refinements in recording and analysis tools are being made.

One example of the potential utility of artifact measures is illustrated in the following two figures, which compare encoded information extracted from artifact potentials with similar information calculated using a mathematical model of the sound processor. Figure 18 shows mapped output levels presented across all channels from a sixteen-channel Clarion High-Resolution processor driving a C-II device with resistive loads. These data were extracted from the multichannel artifact signal (measured at the summing node) using the same artifact processing procedures described in this report. Data are plotted as mapped channel outputs as a function of time for each of the processor's output channels. For comparison, Figure 19 shows the computed mapped outputs across all channels based on a MatLab simulation of the sound processor system. The model results are equally scaled across all channels so that model and measured maximum peak data are equal for channel 4. A visual comparison of the data on a channel-by-channel basis demonstrates the degree of detail that will be available to guide an evaluation of whether a particular implant system is performing as expected.

We will continue to report in future QPRs our progress in evaluating implanted devices. Our next step is to begin collection of data from a larger number of patients using older and newer versions of each of the three major clinical systems.

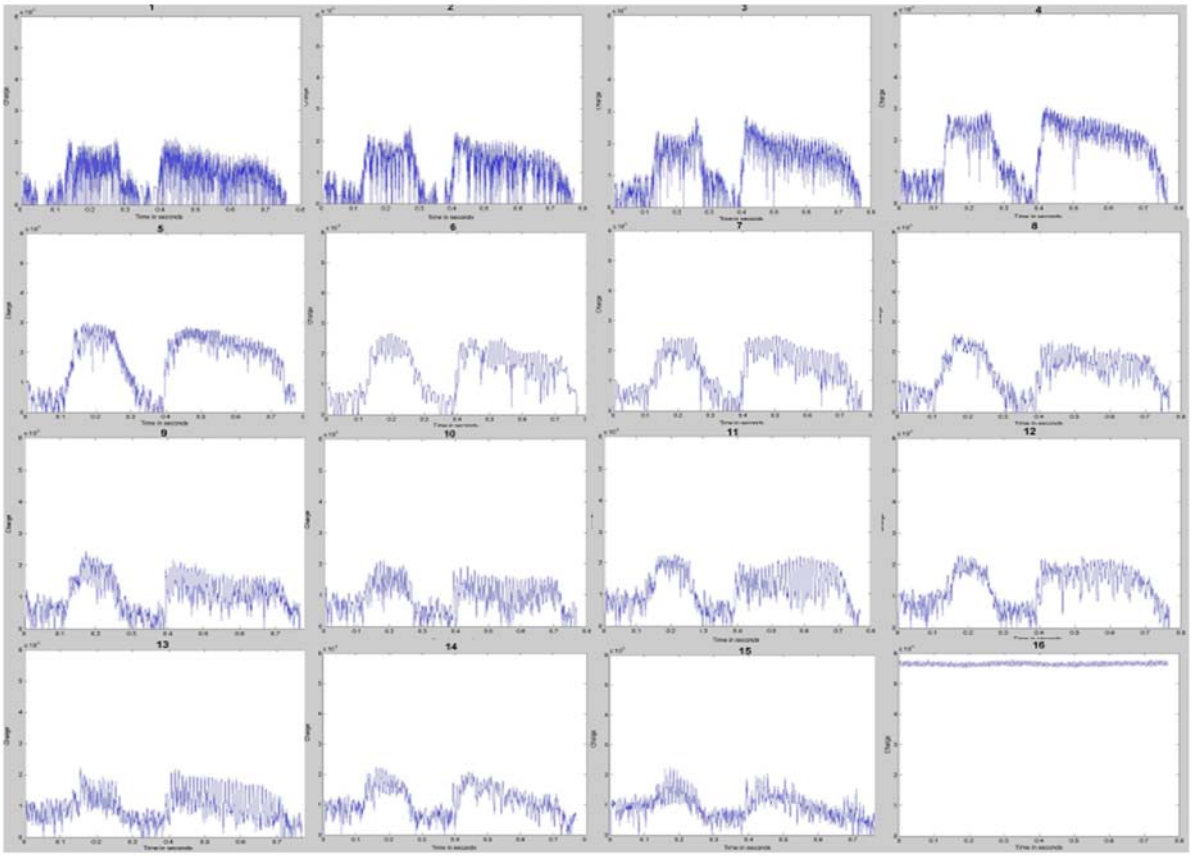

Figure 18. Measured pulse magnitudes versus time for individual channels of a Clarion Hi-Resolution 16-channel processor based on analysis of artifact potentials summed across all channels into a resistive load.

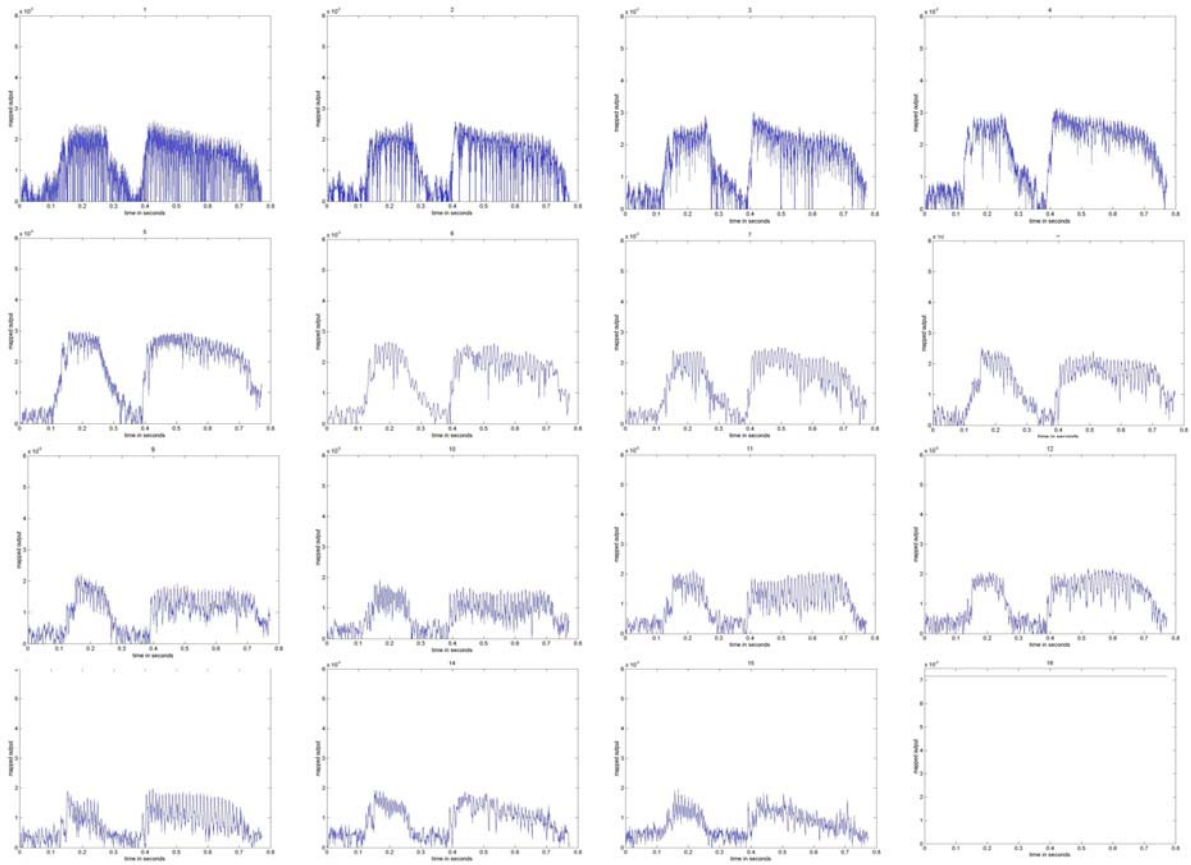

Figure 19. Calculated pulse magnitudes versus time for individual channels of a Clarion Hi-Resolution 16-channel processor based on a MatLab model.

3.0 Future Work

We continue to monitor the relationships of pitch, fusion, ITD-JND and binaural interactions in electrically-evoked brain stem responses and have observed interesting changes with time that will be described in a future QPR. We also continue to monitor the subjects' ability to localize sound and receive speech in quiet and noise using the bilateral, asynchronous sound-processing systems described in previous QPRs. In the next quarter we also plan to begin the testing of bilateral, split-spectrum sound processors. .

We are also continuing our work directed at triphasic stimulation waveforms. We have finished collecting psychophysical measures that compare interaction for biphasic and triphasic stimuli in subjects implanted with the Clarion CII/HiFocus implant system. The results show an advantage for triphasic stimulation. We have implemented a CIS sound-processing strategy employing triphasic carriers in wearable form for one subject and plan to expand that population to at least five subjects in order to investigate whether triphasic stimuli present an advantage to speech reception.

Measurements of channel interaction using intracochlear evoked potentials (IEPs) are continuing using the custom software developed and tested during the first three Quarters in a group of monolaterally-implanted Clarion CII/HiFocus subjects. The primary objectives for collecting these initial data are to (1) better characterize system measurement noise and (2) characterize the magnitude and quality of IEP measures in a pool of subjects with a range of speech-reception performance. We expect to analyze our large body of IEP-based interaction measures in the next quarter and compare them to similar behavioral measures.

4.0 References

Battmer RD, Gnadeberg D, Lehnhardt E and Lenarz T (1994) An integrity test battery for the Nucleus Mini 22 Cochlear Implant System. *Eur Otorhinolaryngol* 251(4): 205-9.

Bordure P, O'Donaghue GM, and Mason S (1996) Electrophysiologic and other objective tests in pediatric implantation. *Ann Otolaryngol Chir Cervicofac* 113(3): 147-54.

Buchman CA, Higgins CA, Cullen R, Pillsbury HC.(2003) Revision cochlear implant surgery in patients with suspected device malfunction. *Otol Neurotol* (in press).

Carter PM (2001) The use of surface potential testing for diagnosing cochlear implant electrode faults and cochlear pathologies. Poster presented at *The Second International Symposium and Workshop on Objective Measures in Cochlear Implantation*, Lyon, France.

Christopher, P (2003) A generic approach to monitoring cochlear implant function, Master's Thesis in Biomedical Engineering, University of North Carolina at Chapel Hill.

Christopher P and Finley C (2003) *In situ* monitoring of the functional operation of cochlear implants – a generic approach, Poster presented at *2003 Conference on Implantable Auditory Prostheses*, Pacific Grove, CA.

Cullington HE and Clarke GP (1997) Integrity testing of cochlear implants in the awake child. *Br J Audiol* 31(4): 247-56.

Eddington DK, Tierney J, Noel V and Whearty M (2002) Speech processors for auditory prostheses, First Quarterly Progress Report, NIH Contract N01-DC-2-1001.

Garnham J, Cope Y and Mason SM (2000) Audit of five–year post-implantation routine integrity tests performed on paediatric cochlear implantees. *Br J Audiol* 34: 285-292.

Heller J, Brehm N, Sinopoli T and Shallop J (1991) Characterization of surface measured potentials from implanted cochlear prostheses. *Proceedings IEEE EMBS Conf* 13: 1907-1908.

Henson AM, Slattery WH III, Luxford WM and Mills DM (1999) Cochlear implant performance after reimplantation. *Am J Otology* 20: 56-64.

Kileny PR, Meiteles LZ, Zwolan TA, and Telian SA (1995) Cochlear implant device failure: diagnosis and management. *Am J Otolology* 16(2): 164-71.

Lehnhardt M, von Wallenberg EL and Brinch JM (2000) reliability of the Nucleus CI22 and CI24M cochlear implants. *Ann Otol Rhinol Laryngol Suppl* 185: 15-16.

Luetje CM and Jjackson K (1997) Cochlear implants in children: What constitutes a complication? *Otolaryngology Head Neck Surg* 117(3 Part 1): 243-247.

Mens LH, Oostendorp T and van den Broek P (1993) Electrode-by-electrode mapping of cochlear implant generated surface potentials: (partial) device failures. In B. Fraysse anf O. Deguine (Eds.), Cochlear Implants: New perspectives. *Advances in Otorhinolaryngology* 48: 475-478.

Mens LH, Oostendorp T and van den Broek P (1994) Identifying electrode failures with cochlear implant generated surface potentials. *Ear Hearing* 15(4): 330-8.

Mens LH and Mulder JJ (2002) Averaged electrode voltages in users of the Clarion cochlear implant device. *Ann Otol rhinol Laryngol* 111(4): 370-5.

Shallop JK (1993) Objective electrophysiological measures from cochlear implant patients. *Ear Hearing* 14(1): 58-63.

Shallop JK, Facer GW, and Peterson A (1999) Neural response telemetry with the Nucleus CI24M cochlear implant. *Laryngoscope* 109(11):1755-9.

Stoddart RL and Cooper HR (1999) electrode complications in 100 adults with multichannel cochlear implants. *J Laryng Otol* 113:18-20.

Truy E, Gallego S, Chanal JM, Collet L, and MorgonA (1998) Correlation between electrical auditory brainstem response and perceptual thresholds in digisonic cochlear implant users. *Laryngoscope* 108(4 Pt 1): 554-9.

von Wallenberg EL and Brinch JM (1995) Cochlear implant reliability. *Ann Otol Rhinol Laryngol Suppl* 104(suppl 166): 441-3.